Journal of Dental Research
2016, Vol. 95(5) 588–596

DOI: 10.1177/0022034515625939
jdr.sagepub.com

Evidence for Bicarbonate Secretion by Ameloblasts in a Novel Cellular Model

E. Bori[1], J. Guo[2], R. Rácz[1], B. Burghardt[1], A. Földes[1], B. Kerémi[1], H. Harada[3], M.C. Steward[4], P. Den Besten[5], A.L.J.J. Bronckers[2], and G. Varga[1]

Abstract

Formation and growth of hydroxyapatite crystals during amelogenesis generate a large number of protons that must be neutralized, presumably by HCO_3^- ions transported from ameloblasts into the developing enamel matrix. Ameloblasts express a number of transporters and channels known to be involved in HCO_3^- transport in other epithelia. However, to date, there is no functional evidence for HCO_3^- transport in these cells. To address questions related to HCO_3^- export from ameloblasts, we have developed a polarized 2-dimensional culture system for HAT-7 cells, a rat cell line of ameloblast origin. HAT-7 cells were seeded onto Transwell permeable filters. Transepithelial resistance was measured as a function of time, and the expression of transporters and tight junction proteins was investigated by conventional and quantitative reverse transcription polymerase chain reaction. Intracellular pH regulation and HCO_3^- transport were assessed by microfluorometry. HAT-7 cells formed epithelial layers with measureable transepithelial resistance on Transwell permeable supports and expressed claudin-1, claudin-4, and claudin-8—key proteins for tight junction formation. Transport proteins previously described in maturation ameloblasts were also present in HAT-7 cells. Microfluorometry showed that the HAT-7 cells were polarized with a high apical membrane CO_2 permeability and vigorous basolateral HCO_3^- uptake, which was sensitive to Na^+ withdrawal, to the carbonic anhydrase inhibitor acetazolamide and to H_2DIDS inhibition. Measurements of transepithelial HCO_3^- transport showed a marked increase in response to Ca^{2+}- and cAMP-mobilizing stimuli. Collectively, 2-dimensional HAT-7 cell cultures on permeable supports 1) form tight junctions, 2) express typical tight junction proteins and electrolyte transporters, 3) are functionally polarized, and 4) can accumulate HCO_3^- ions from the basolateral side and secrete them at the apical membrane. These studies provide evidence for a regulated, vectorial, basolateral-to-apical bicarbonate transport in polarized HAT-7 cells. We therefore propose that the HAT-7 cell line is a useful functional model for studying electrolyte transport by ameloblasts.

Keywords: dental enamel, in vitro techniques, ion transport, cytophotometry, fluorescent dyes, tissue engineering

Introduction

Ameloblasts are electrolyte-transporting epithelial cells that transport calcium and phosphate ions, the principal building blocks of hydroxyapatite crystals, into the enamel space. Formation of hydroxyapatite during the maturation stage of amelogenesis generates a large quantity of protons, and to sustain crystal growth, these protons need to be neutralized (Smith 1998; Lacruz et al. 2013; Jalali et al. 2014). To buffer the pH in the enamel space, ameloblasts seem to have the molecular machinery to secrete HCO_3^- ions into the enamel space. Maturation ameloblasts express carbonic anhydrase 2 and 6 (*Car2, Car6*), the Cl^--HCO_3^- exchanger 2 (*Slc4a2/Ae2*), Na^+-HCO_3^- cotransporter (*Slc4a4/Nbce1*), Na^+-H^+ exchanger 1 (*Slc9a1/Nhe1*), cystic fibrosis transmembrane conductance regulator (*Cftr*), *Slc26a4/pendrin, Slc26A3/Dra*, and *Slc26a6/Pat1* (Bronckers et al. 2011; Lacruz et al. 2013; Jalali et al. 2014; Jalali et al. 2015). Additional mechanisms probably also participate in extracellular pH control. Recent studies indicated the likely involvement of active proton transport and the importance of tight junction (TJ) proteins in enamel formation (Josephsen et al. 2010; Damkier et al. 2014; Bardet et al. 2016). Studies on loss of function of several of these proteins have indicated their involvement in mineralization (Smith 1998; Lyaruu et al. 2008; Bronckers et al. 2011; Lacruz et al. 2013; Bronckers et al. 2015). At present, all of the available

[1]Department of Oral Biology, Semmelweis University, Budapest, Hungary
[2]Department of Oral Cell Biology, Academic Centre for Dentistry Amsterdam, University of Amsterdam and VU University Amsterdam, MOVE Research Institute, Amsterdam, Netherlands
[3]Department of Anatomy, Division of Developmental Biology and Regenerative Medicine, Iwate Medical University, Iwate, Japan
[4]Faculty of Life Sciences, The University of Manchester, Manchester, UK
[5]Department of Orofacial Sciences, University of California, San Francisco, CA, USA

A supplemental appendix to this article is published electronically only at http://jdr.sagepub.com/supplemental.

Corresponding Author:
G. Varga, H-1089 Budapest, Nagyvárad tér 4, Hungary.
Email: varga.gabor@dent.semmelweis-univ.hu

information about pH regulation–related electrolyte transport by ameloblasts is based solely on immunohistochemistry, tracer and staining techniques, and expression studies without any functional corroboration. Consequently, mechanistic models such as these are purely hypothetical, and there is a need for suitable experimental models to enable functional measurements of transport activity.

HAT-7 is a dental epithelial cell line derived from the cervical loop epithelium of a rat incisor, established in 2002 (Kawano et al. 2002). Immunocytochemical studies showed that HAT-7 cells exhibit several ameloblast characteristics, including the expression of amelogenin and ameloblastin (Kawano et al. 2002) and also maturation-stage ameloblast markers such as kallikrein-4 (*Klk4*) and amelotin. However all of these studies have been restricted to expression profiling (Harada et al. 2006; Yoshizaki et al. 2008; Matsumoto et al. 2011; Zheng et al. 2013). The purpose of the present study was 1) to establish confluent monolayers of HAT-7 cells on permeable supports, 2) to characterize gene expression of TJ and electrolyte transport proteins, and 3) to assess the functional polarization of monolayers and their capacity for basolateral to apical HCO_3^- transport.

Materials and Methods

Cell Culture

HAT-7 cells were grown on permeable polyester Transwell culture inserts with 0.4-μm pore size and 1.12-cm^2 surface area (Corning Inc., Corning, NY, USA) and cultured in 3 media:

- *C:* control medium consisting of DMEM/F12 (Sigma-Aldrich, St. Louis, MO, USA) with 10% HyClone fetal bovine serum (Thermo Scientific, Waltham, MA, USA)
- *D:* differentiation medium, the same medium but supplemented with $CaCl_2$ (final concentration 2.1 mM) and 10^{-5} mM dexamethasone (Sigma-Aldrich; Arakaki et al. 2012)
- *H:* hepato-STIM medium, a commercially available epithelial selection medium effectively used for primary salivary gland cultures (Szlavik et al. 2008; Hegyesi et al. 2015)

All media contained 100 U/mL of penicillin and 10 μg/mL of streptomycin (Sigma-Aldrich), and cells were grown in a humidified atmosphere containing 5% CO_2 at 37 °C.

Measurement of Transepithelial Electrical Resistance, Immunocytochemistry, RT-PCR, RT-qPCR, Microfluorometry, and Statistical Analysis

The following were performed as described in the Appendix: transepithelial electrical resistance (TER) of cells on Transwell, immunocytochemical imaging for identification of cell-specific proteins (Bronckers et al. 2015; Jalali et al. 2015), methods identifying TJ proteins and expected electrolyte transporters by applying standard semiquantitative and quantitative polymerase chain reaction technologies to amplify the mRNA (Hegyesi et al. 2015), microfluorometric measurements, and statistical analyses (Szucs et al. 2006).

Results

Morphology and Immunocytochemistry of HAT-7 Cells

HAT-7 cell cultures showed morphology and growth characteristics similar to their original description (Kawano et al. 2002). The cells covered the Transwell surface and reached confluence in 2 to 3 d regardless of choice of culture medium (Fig. 1a, b). Transverse sections showed that the cells were either very flat or cuboidal and mostly formed a single layer with small regions of ≥2 layers (Fig. 1). Immunostaining for zonula occludens-1 (TJP1/ZO1; Fig. 1c) resulted in widespread positive labeling, while application of normal nonimmune rabbit IgG as control showed no labeling (Fig. 1h). Positive immunostaining for maturation-stage markers such as *Klk4* (Fig. 1d, e) and amelotin (Fig. 1g) was observed both en face and in transverse sections, suggesting that HAT-7 cells exhibit a maturation-stage ameloblast phenotype.

Positive staining for SLC4A4/NBCe1, SLC4A2/AE2, SLC26A4/pendrin, SLC26A6/PAT1, CFTR, and CAR2 on transverse sections revealed the presence of all 6 proteins involved in HCO_3^- secretion (Fig. 1i–r). There were no qualitative differences in the expression patterns of these proteins in HAT-7 cells (data not shown) grown in the D and H media that we used for further experimentation.

TER, TJ Formation, and Transporter Expression

To check for functional polarization of the confluent layers of HAT-7 cells, TER was measured. There were striking differences in the TER value when different media were used. TER values were lowest in cells grown in C medium and highest in H medium (Fig. 2A). Resistance curves typically reached a peak value on the fourth or fifth day and declined to lower plateau phase by the seventh day. The peak values show that the TJs are fully formed, and the lower plateau phase that follows reflects the increasing TJ density as the cell numbers increase.

Using RT-PCR (reverse transcription polymerase chain reaction), we found expression of Tjp1/Zo1 and claudins (*Cldn1, Cldn4*, and *Cldn8*) at mRNA level in every HAT-7 sample, regardless of whether they were grown on plastic or on porous Transwell membranes (Fig. 2B). Quantitative polymerase chain reaction data normalized to Rplpo (Fig. 2C) revealed that claudins were at least doubled in the Transwell groups (C, D, and H media) as compared with their expression on plastic. The culture medium also influenced the expression pattern. The greatest difference was observed in *Cldn8* expression, where the relative quantity (normalized to the plastic group samples) ranged from 7.9 ± 0.4 in C medium to 22.1 ± 4.2 in H. In the case of *Cldn1* and *Cldn4*, expression primarily

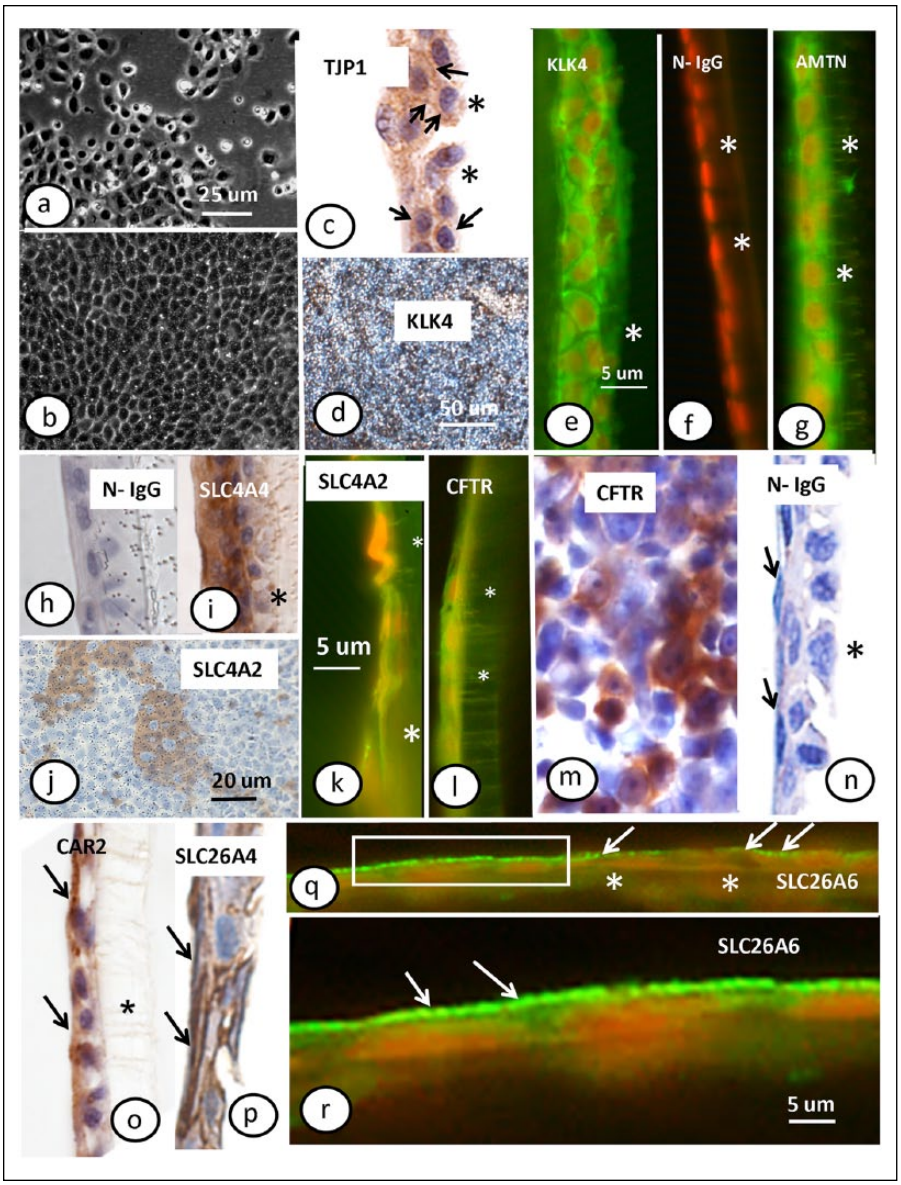

Figure 1. Morphology and immunocytochemistry of HAT-7 cells. HAT-7 cells grown on a plastic culture plate (**a**) and Transwell membrane (**b**); phase contrast. Immunocytochemical localization of (**c**) tight junction protein 1 (TJP1/ZO1, zonula occludens-1; arrows indicate at weakly stained plasma membrane); (**d**, **e**) kallikrein 4 (KLK4) with (**f**) normal IgG control; (**g**) amelotin (AMTN); (**h**) normal IgG control with cuboic surface cells; (**i**) Na^+-HCO_3^- cotransporter-e1 (SLC4A4/NBCe1); (**j**) anion exchanger 2 (SLC4A2/AE2) in top view and cross section (**k**); (**l**, **m**) cystic fibrosis transmembrane conductance regulator (CFTR) in cross section (l) or top view (m); (**n**) normal IgG control with flattened surface cells (arrows refer to the apical surface of the cells); (**o**) carbonic anhydrase type 2 (CAR2; arrows indicate surface cells with positive staining in apical part); (**p**) SLC26A4/pendrin (arrows point at surface staining); (**q**, **r**) SLC26A6/PAT1. Panels a, b, d, j, m: top views; all others: cross sections. Arrows in panels q and r indicate positive reaction in the membrane facing the culture medium. (q) The reaction is interrupted at the right half and continuous at the left half. (r) A higher magnification of boxed area at the left side. Immunofluorescence: green in e to g, k, l, q, r with nuclei in orange; peroxidase: brown in in d, h, j, m to p with nuclei in blue. Asterisks show position of Transwell membrane. Panels a to c, e, h to l, o, p: hepato-STIM culture medium; d to g, m, q, r: differentiation culture medium. Original magnifications: a, b (100×); c to i, k to p, r (400×); d (50×); q (200×). This figure is available in color online at http://jdr.sagepub.com.

depended on the surface used but not on the culture medium (Fig. 2C). The expression of *Tjp1/Zo1* was increased in C and D media but not in H medium. Likewise, the expression of maturation ameloblast-specific *Klk4* considerably increased in HAT-7 cells cultivated on Transwells in C and D media but not in H medium (Fig. 2D).

Key electrolyte transporters/channels such as *Slc9a1/Nhe1, Slc4 a2/Ae2, Slc4a4/Nbce1, Slc26a4/pendrin*, and *Cftr* were all expressed in HAT-7 cells (Fig. 2D), although at variable levels. Similar to this, the cytoplasmic carbonic anhydrase *Car2* isoform highly expressed in maturation ameloblasts in situ could be also detected (Fig. 2D). Quantitative polymerase chain reaction experiments showed that the expression of *Slc 9a1/Nhe1, Slc4a2/Ae2, Slc4a4/Nbce1, Slc26a4/pendrin* significantly increased in cells cultivated on Transwells both in C and D media but not in H medium (Fig. 2D). No significant changes were observed for *Cftr*, while *Car2* expression increased only in cells cultivated in H medium on Transwells (Fig. 2D).

Functional Polarization of HAT-7 Cells

Although culture in H medium yielded the highest TER values and the highest levels of expression of TJ proteins, preliminary functional experiments indicated that in this medium, HAT-7 cells produced more variable and less consistent results (data not shown). Therefore, we continued our studies with HAT-7 cells cultivated in D medium, which produced moderate TER values and behaved consistently in microfluorometric experiments.

Bicarbonate and CO_2 membrane permeabilities were investigated by unilaterally exposing the HAT-7 cells to HCO_3^-/CO_2 (Fig. 3). After perfusing the apical and basolateral sides of the cells with the HCO_3^--free HEPES-buffered solution, apical perfusion was switched to the HCO_3^-/CO_2 solution. A rapid acidification of intracellular pH (pH_i) occurred as a result of CO_2 diffusion into the cells (Fig. 3A). Following this, pH_i reached a new level and remained there until the HEPES solution was restored at the apical side. This induced a rapid alkalinization of pH_i toward the resting value as a result

of the diffusion of CO_2 out of the cells (Fig. 3A). When the same change, from HEPES to HCO_3^-/CO_2, was performed on the basolateral side, pH_i increased rapidly and reversibly showing the uptake of HCO_3^- ions (Fig. 3A).

Inhibition of Basolateral HCO_3^- Uptake by HAT-7 Cells

To test whether anion transporters are responsible for HCO_3^- uptake, we repeated the switch from HEPES to HCO_3^-/CO_2 in the absence and the presence of H_2DIDS, an inhibitor of anion transport. Repeated switch from HEPES to HCO_3^-/CO_2 without inhibitor application resulted in no change of alkalinization dynamics (Fig. 3B, E). When H_2DIDS was added, the alkalinization was smaller and slower than in controls (Fig. 3C, E), indicating that a basolateral HCO_3^- transporter, most probably NBCe1/SLC4A4, has an important role in HCO_3^- uptake. To investigate the role of carbonic anhydrase in intracellular HCO_3^- accumulation, we used acetazolamide (100 μM), a membrane-permeable carbonic anhydrase inhibitor. In the presence of acetazolamide, the alkalinization was again inhibited, suggesting that carbonic anhydrase also contributes to HCO_3^- accumulation (Fig. 3D, E).

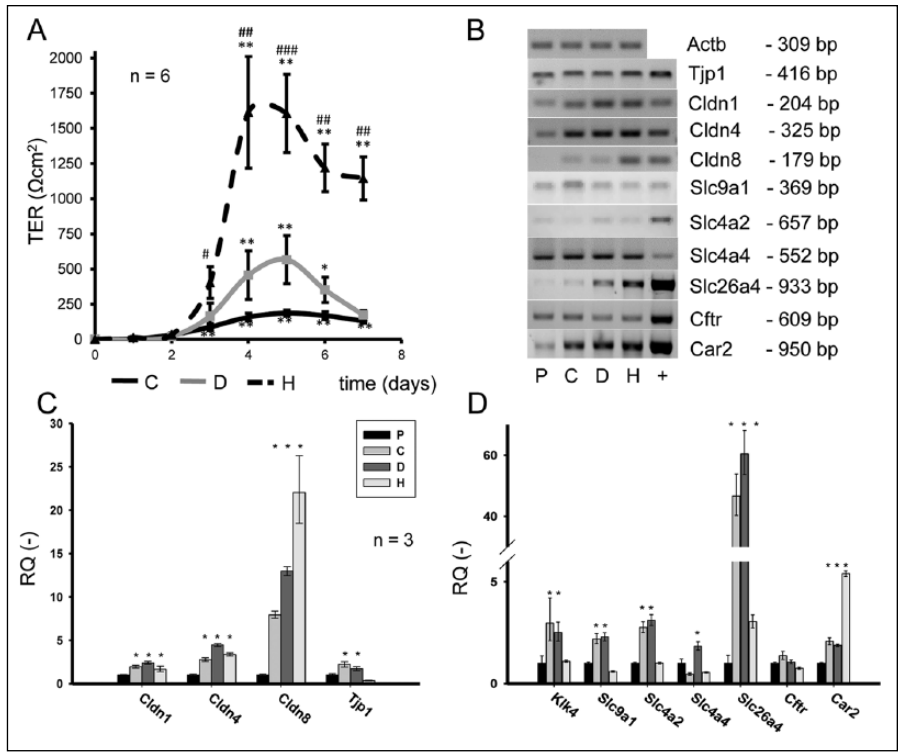

Figure 2. Transepithelial resistance, tight junction formation in HAT-7 cells cultured in different media. (**A**) Transepithelial resistance (TER) of HAT-7 cells cultured on Transwell membranes for 7 d. Cells were cultured in control (C), differentiation (D), or Hepato-STIM (H) medium ($n = 6$). Significant changes in TER compared with day 0: $^*P < 0.05$, $^{**}P < 0.01$, $^{***}P < 0.005$. Significant differences in TER compared with same-day control: $^{\#}P < 0.05$, $^{\#\#}P < 0.01$, $^{\#\#\#}P < 0.005$. (**B**) Conventional RT-PCR (reverse transcription polymerase chain reaction), data showing mRNA expression of *Tjp1, Cldn1, Cldn2, Cldn8, Slc9a1/Nhe1, Slc4a2/Ae2, Slc4a4/Nbce1, Slc26a4/pendrin, Cftr*, and *Car2* genes in HAT-7 cells cultured on Petri dishes in control medium (plastic [P]) and on Transwells in C, D, and H media. Kidney and ileum mRNAs were used as positive controls (+). (**C**) Quantitative RT-PCR data showing expression of tight junction–specific *Cldn1, Cldn2, Cldn8*, and *Tjp1/Zo1* genes in HAT-7 cells grown on Transwells in C, D, and H media, normalized to their expression in cells grown on plastic in C medium ($n = 3$). (**D**) Quantitative RT-PCR data showing expression of maturation phase ameloblast marker gene *Klk4*; electrolyte transporters *Slc9a1/Nhe1, Slc4a2/Ae2, Slc4a4/Nbce1*, and *Slc26a4/pendrin*; and *Cftr* and *Car2* genes in HAT-7 cells treated as described above ($n = 3$). Significant changes in expression compared with cells grown on P surface: $^*P < 0.05$.

To identify the mechanism of HCO_3^- transport across the basolateral membrane, we next used the NH_4^+ prepulse technique. As expected, bilateral application of a 20mM NH_4^+ pulse caused a transient intracellular alkalinization, followed by a marked acidification (Fig. 4). In the standard HCO_3^-/CO_2 solution, pH_i recovered gradually from the acidification, most probably as a result of H^+ extrusion by Na^+-H^+ exchange and HCO_3^- uptake by Na^+-HCO_3^- cotransport (data not shown). However, when the NH_4^+ pulse was immediately followed by bilateral substitution of Na^+ with the nontransported cation $NMDG^+$, the recovery of pH_i was completely abolished (Fig. 4A). Restoration of Na^+ led to a rapid recovery in pH_i. This indicates that the basolateral transport mechanism is Na^+ dependent and does not involve proton pump activity. It is therefore most likely to be mediated by NBCe1/SLC4A4 and/or NHE/SLC9A1 (Fig. 4A, B). To test this hypothesis, 300μM amiloride and 500μM H_2DIDS were applied to suppress basolateral NHE1/SLC9A1 and NBCe1/SLC4A4 activities, respectively, immediately after Na^+ restoration (Fig. 4B). The recovery of pH_i following the NH_4^+ pulse was reduced by about 85% in the presence of the inhibitors (Fig. 4B, C) in support of our hypothesis. To further confirm the identity of Na^+-H^+ exchange cariporide, a highly selective NHE1/SLC9A1 inhibitor was used instead of amiloride (Harguindey et al. 2013). These experiments revealed that 10μM cariporide was as effective as amiloride (Fig. 4D).

Bicarbonate Secretion

The ability to block HCO_3^- uptake across the basolateral membrane allows us to estimate the rate of HCO_3^- secretion across the apical membrane. Following basolateral blockade, HCO_3^- secretion continues at the apical membrane, and pH_i falls as a result. The initial acidification rate, which is a measure of HCO_3^- secretion, was estimated with unstimulated HAT-7 cells (Fig. 5A, B) and also during stimulation with ATP (50 μM) to mobilize intracellular Ca^{2+} (Fig. 5C, E) or forskolin (10 μM) and IBMX (500 μM) to elevate intracellular cAMP (Fig. 5D) or the 3 combined (Fig. 5F). The initial acidification rates,

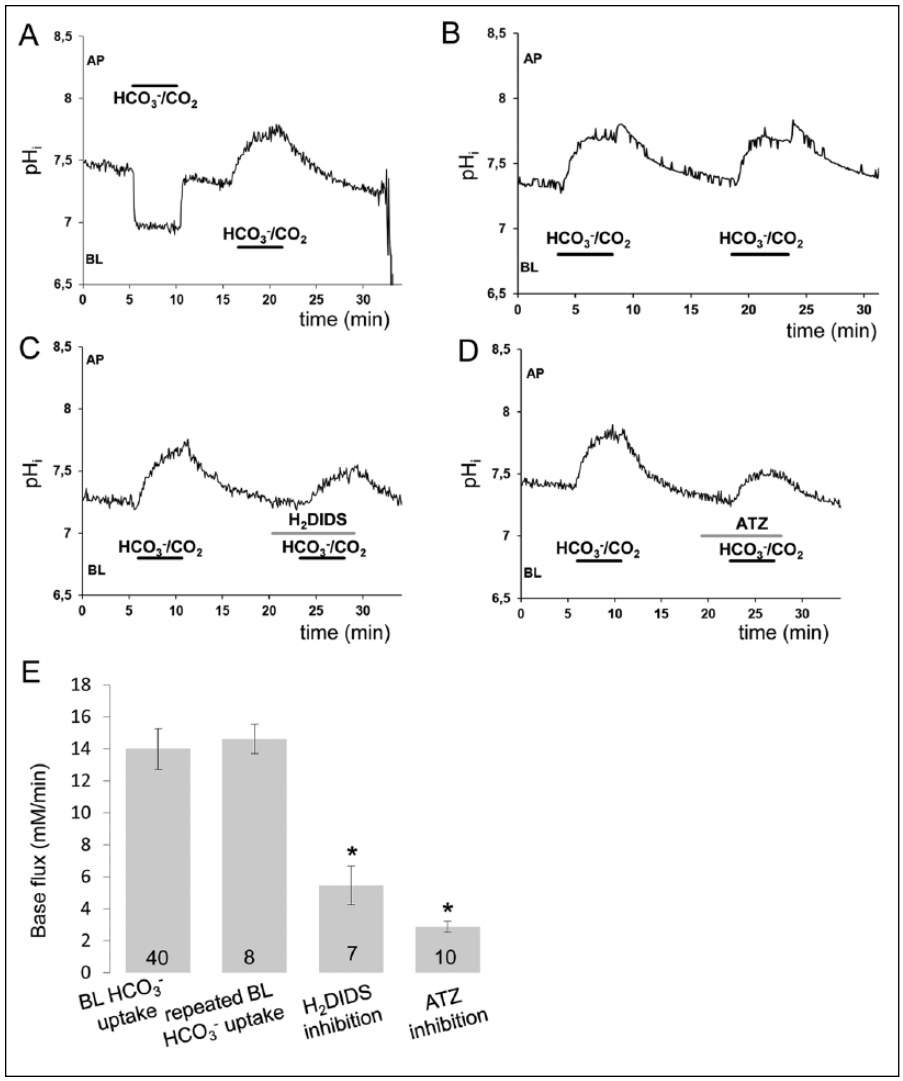

Figure 3. Functional polarization and bicarbonate uptake by HAT-7 cells. (**A**) Changes in intracellular pH (pH_i) in HAT-7 cells grown on Transwells in differentiation medium and bathed initially in HCO_3^-/CO_2-free, HEPES-buffered solution. Apical (AP) and basolateral (BL) surfaces were separately exposed to HCO_3^-/CO_2-buffered perfusate for 5 min. (**B**, **C**) Changes in pH_i evoked by basolateral exposure to HCO_3^-/CO_2 in the absence and presence of H_2DIDS (500 µM). (**D**) Changes in pH_i evoked by basolateral exposure to HCO_3^-/CO_2 in response to acetazolamide (ATZ; 100 µM). (**E**) Mean base fluxes (± SEM) calculated from the initial rates of increase in pH_i following basolateral exposure to HCO_3^-/CO_2 in the presence and absence of the inhibitors (n = 7 to 40). *P < 0.05 compared with control.

expressed as base fluxes, are summarized in Figure 5A. In the absence of stimulation, the base flux was very low (Fig. 5B), suggesting only a low level of basal HCO_3^- secretion. Apical application of ATP had no significant effect (Fig. 5A, C), but basolateral ATP caused a small but significant increase (Fig. 5C), as did apical forskolin and IBMX (Fig. 5E). The largest response was seen when basolateral ATP and apical forskolin and IBMX were applied simultaneously (Fig. 5F), providing clear evidence that HAT-7 cells are capable of vectorial HCO_3^- secretion in a basal to apical direction. When amiloride was replaced by the selective NHE1/SLC9A1 antagonist cariporide, simultaneous ATP, forskolin, and IBMX administration yielded an initial base flux of 1.77 ± 0.24 mM/min, a similar value found during amiloride application.

Discussion

A major finding of the present work is that ameloblast-derived HAT-7 cells are able to form polarized confluent monolayers on permeable supports and develop measurable TER. We also found expression of *Cldn1, Cldn4, Cldn8*, and *Tjp1/Zo1*, which indicates the presence of mature TJs (Figs. 1, 2). These are a prerequisite for vectorial electrolyte secretion by restricting free transepithelial ion movements but permitting passage of certain ions between the cells (Melvin et al. 2005; Steward et al. 2005; Hou 2014). The higher level of *Cldn8* expression in the H medium compared with the D and C media is in line with our observation that TER was highest in the H medium, modest in the D medium, and very low in the C medium (Amasheh et al. 2009). The data are also in accordance with previous studies (Colegio et al. 2002; Amasheh et al. 2009; Lal-Nag and Morin 2009) showing the expression of *Cldn1, Cldn4*, and *Cldn8* in maturation-stage ameloblasts (Inai et al. 2008; Hata et al. 2010). In spite of the fact that H medium induced the highest TER and the highest expression of claudins, functional measurements of electrolyte transport with H medium were erratic and inconsistent, and transporter expression was diminished as compared with cells in C or D medium. In many Cl^-- and HCO_3^--secreting epithelia (e.g., salivary acini and pancreatic ducts), the TJs have to be relatively "leaky" to support the necessary paracellular transport of Na^+ ions (Melvin et al. 2005; Steward et al. 2005; Hou 2014). If HCO_3^- secretion by ameloblasts is accompanied by paracellular Na^+ transport, we would anticipate that a relatively leaky junctional phenotype would be more likely than the very high resistances observed in the cells grown in H medium—hence, our choice of the D medium for all subsequent studies.

Previous studies indicated that *Slc9a1/Nhe1, Slc4a2/Ae2, Slc4a4/Nbce1, Slc26a4/pendrin*, and *Cftr* are expressed by ameloblasts and are necessary for intracellular and extracellular pH regulation (Bronckers et al. 2011; Lacruz et al. 2013;

Jalali et al. 2014). Among carbonic anhydrases, the cytoplasmic *Car2* isoform is dominant, although others have been described (Lacruz, Smith, Moffatt, et al. 2012; Reibring et al. 2014). The fact that HAT-7 cells grown on Transwell filters express maturation-stage ameloblast-specific markers (including *Slc9a1/Nhe1, Slc4a2/Ae2, Slc4a4/Nbce1, Slc26a4/pendrin, Cftr*, and *Car2*) suggests that this cell line is suitable as an experimental model for studying ameloblast acid/base transport (Fig. 2).

Our results demonstrate that HAT-7 cells are functionally polarized with 1) an apical membrane that is highly permeable to CO_2 but does not take up HCO_3^- and 2) a basolateral membrane that has a lower permeability to CO_2 but is capable of vigorous HCO_3^- uptake (Fig. 3). This is similar to other HCO_3^--secreting epithelia, such as guinea pig pancreatic duct (Ishiguro et al. 2000) and the human CFPAC cells (Rakonczay et al. 2006). It is also consistent with the suggestion that maturation-stage ameloblasts are equipped to secrete HCO_3^- to neutralize the acidity generated at the apical border of ameloblasts during hydroxyapatite formation (Smith 1998; Lacruz et al. 2013; Jalali et al. 2014).

The 2 most likely pathways for basolateral HCO_3^- uptake in ameloblasts are by Na^+-HCO_3^- cotransport and by CO_2 diffusion into the cells, with carbonic anhydrase catalyzing its conversion into HCO_3^- ions and protons (Lacruz et al. 2013; Jalali et al. 2014). In our conditions, a substantial proportion of the basolateral HCO_3^- uptake was Na^+ dependent and inhibited by H_2DIDS and therefore most likely due to the action of the ubiquitously expressed NBCe1/SLC4A4 cotransporter. Again there are parallels with the pancreatic duct epithelium, where NBCe1/SLC4A4 makes a major contribution to the basolateral uptake of HCO_3^- (Ishiguro et al. 1996). The application of the membrane-permeable carbonic anhydrase inhibitor acetazolamide also partially inhibited the basolateral base flux in HAT-7 cells, suggesting that the alternative mechanism is present and presumably dependent on H^+ extrusion via a basolateral Na^+-H^+ exchanger (Fig. 3). Among the large number of different isoenzymes in the carbonic anhydrase gene family, the dominant isoform in ameloblasts is *Car2* (Lacruz et al. 2010; Reibring et al. 2014), the isoform that we found to be expressed in HAT-7 cells.

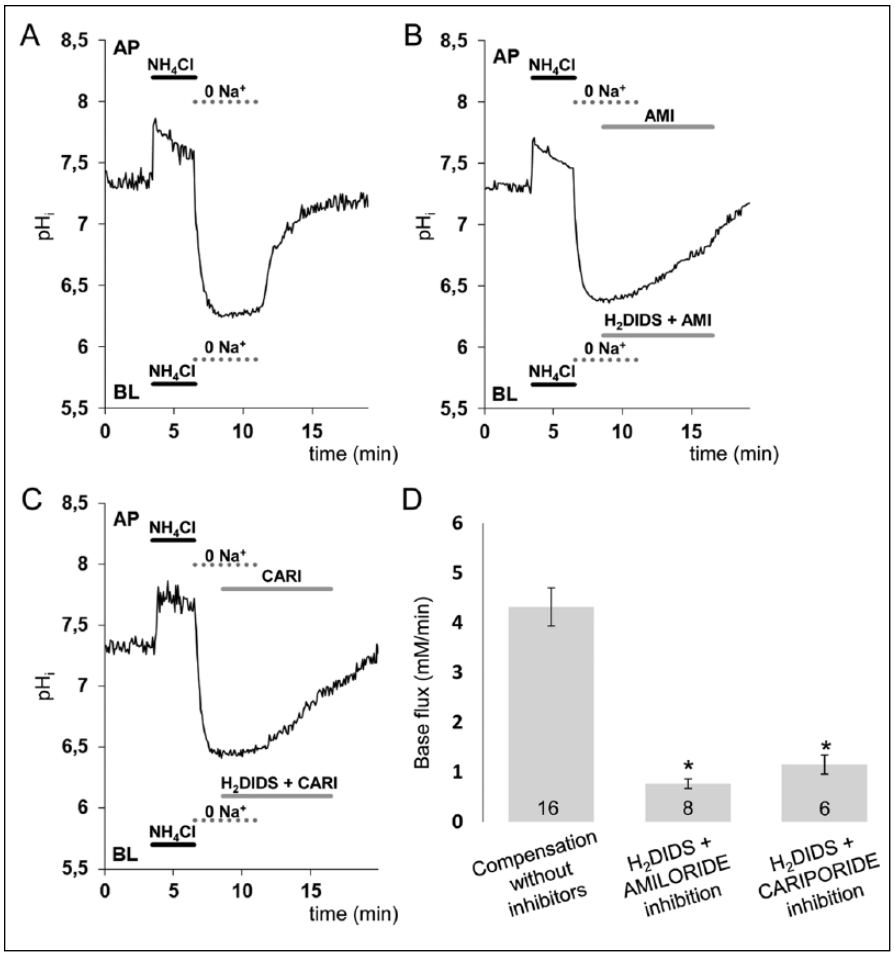

Figure 4. Recovery of intracellular pH (pH_i) in HAT-7 cells exposed to an acid load in the presence of HCO_3^-/ CO_2. HAT-7 cells grown on Transwell supports in differentiation medium were exposed bilaterally to 20mM NH_4^+, followed by bilateral substitution of Na^+ with $NMDG^+$. (**A**) Recovery of pH_i following bilateral restoration of extracellular Na^+. (**B**) Inhibition of pH_i recovery following restoration of Na^+ in the presence of basolateral (BL) H_2DIDS (500 µM) and amiloride (300 µM). Amiloride was also included in the apical (AP) perfusate to inhibit any apical NHE activity. (**C**) Similar inhibitory experiment is shown as in panel B, but amiloride was replaced by the specific inhibitor cariporide (10 µM) to selectively block the NHE1/SLC9A1 antiport. (**D**) Mean base fluxes (± SEM) calculated from the initial rates of increase in pH_i following restoration of Na^+ in the presence and absence of the inhibitors (n = 8 to 10). *P < 0.05 compared with control.

Our NH_4^+ pulse experiments showed that removal of Na^+ from the bathing solution fully prevented the pH_i recovery of the HAT-7 cells following acidification (Fig. 4), similar to other HCO_3^--secreting epithelia (Ishiguro et al. 1996; Szucs et al. 2006; Demeter et al. 2009). Application of 300µM amiloride and 500µM H_2DIDS to inhibit NHE1/SLC9A1 and NBCe1/SLC4A4 (Ishiguro et al. 1996; Demeter et al. 2009; Lee et al. 2012) resulted in an approximately 85% inhibition of the recovery rate from the acid load, suggesting that NHE1/SLC9A1 and NBCe1/SLC4A4 transporters are jointly responsible for most of the basolateral HCO_3^- uptake. This was further confirmed when amiloride was replaced by the NHE1/SLC9A1 selective cariporide (Harguindey et al. 2013).

As H_2DIDS and amiloride blocked most of the basolateral uptake of HCO_3^-, we could use a relatively simple fluorometric method to test whether HAT-7 cells are able to achieve vectorial

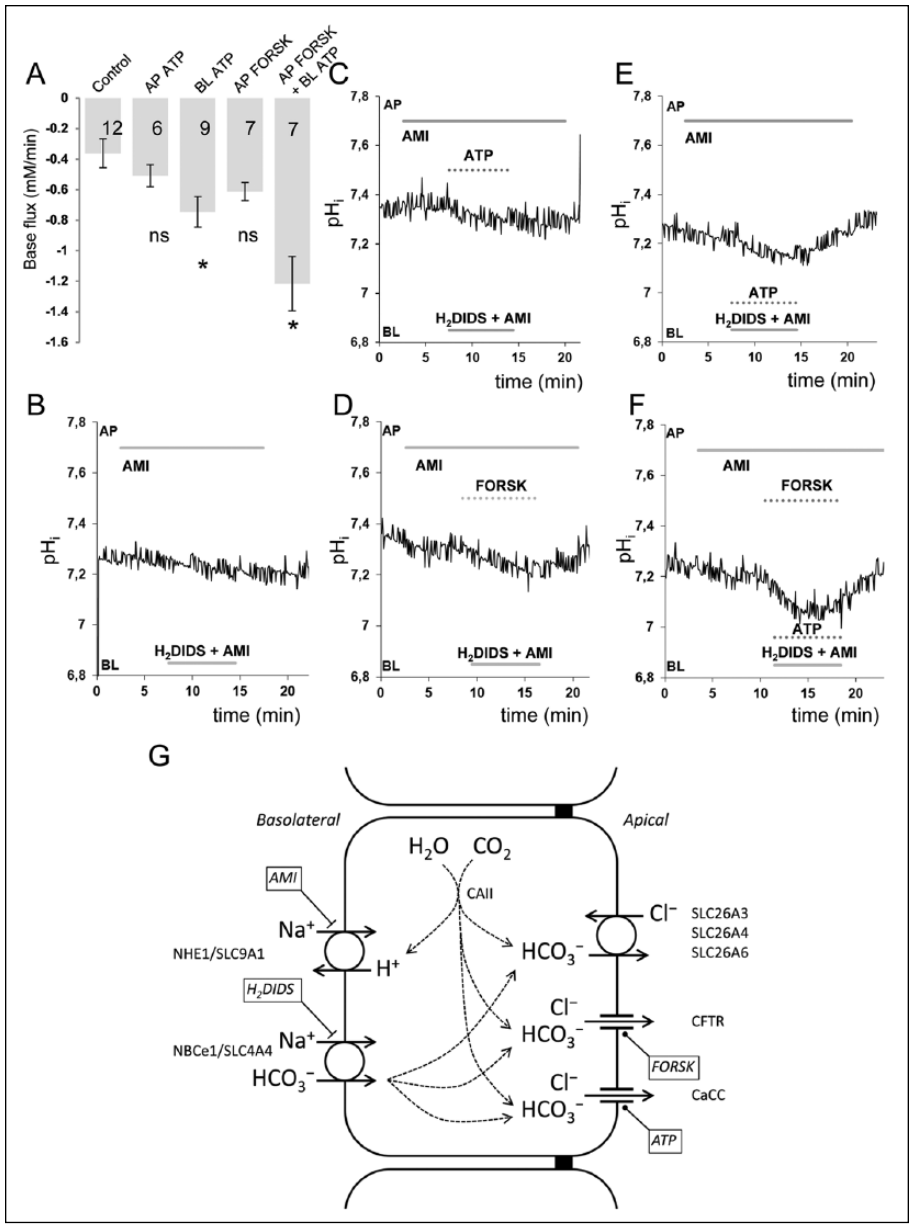

Figure 5. Intracellular acidification evoked in HAT-7 cells by inhibition of basolateral HCO_3^- uptake in the presence and absence of ATP and forskolin. Basolateral HCO_3^- uptake in HAT-7 cells grown on Transwells in differentiation medium was inhibited by simultaneous basolateral (BL) application of 500μM H_2DIDS and 300μM amiloride (AMI). AMI was also included in the apical (AP) perfusate to inhibit any apical NHE1/SLC9A1 activity. (**A**) Mean base fluxes (± SEM) calculated from the initial rates of decrease in intracellular pH (pH_i) following application of basolateral H_2DIDS and AMI in the presence and absence of ATP and/or forskolin and IBMX (FORSK). *$P < 0.05$ compared with control. Representative pH_i traces obtained in unstimulated control conditions (**B**) and in the presence of (**C**) apical ATP (50 μM), (**D**) apical forskolin (10 μM) and IBMX (500 μM), (**E**) basolateral ATP (50 μM), and (**F**) apical forskolin (10 μM) and IBMX (500 μM) in combination with basolateral ATP (50 μM). (**G**) Schematic depiction of the proposed mechanism of vectorial bicarbonate transport of HAT-7 cells, exhibiting the major transporters and channels involved in the process.

HCO_3^- secretion. In secretory epithelia, HCO_3^- entry across the basolateral membrane is closely coupled to HCO_3^- efflux across the luminal membrane (Ishiguro et al. 1996; Szucs et al. 2006; Demeter et al. 2009). Therefore, when HCO_3^- entry is blocked by transport inhibitors, the continuing efflux of HCO_3^- across the luminal membrane leads to a fall in pH_i. The initial rate of fall in pH_i therefore serves as an index of instantaneous HCO_3^- efflux across the apical membrane. When we applied a combination of NHE1/SLC9A1 and NBCe1/SLC4A4 inhibitors to unstimulated HAT-7 cells, we observed a slow acidification due to apical HCO_3^- secretion, but this was more pronounced when the cells were stimulated (Fig. 5). Extracellular ATP, a bioactive molecule acting through purinergic receptors to raise intracellular Ca^{2+} (Schwiebert and Zsembery 2003), stimulated HCO_3^- transport when applied to the basolateral but not to the apical side. In other secretory epithelia, the differing effects of apical and basolateral ATP on HCO_3^- secretion are well documented (Schwiebert and Zsembery 2003; Szucs et al. 2006; Baggaley et al. 2007; Demeter et al. 2009). The present work raises the possibility that extracellular ATP could be an important regulator of ameloblast function, most probably acting via calcium-activated chloride channels recently identified in maturation-stage ameloblasts using protein expression assays (Lacruz, Smith, Bringas, et al. 2012). Forskolin, which activates the cAMP/protein kinase A pathway, strongly potentiated the effect of ATP, most probably by opening CFTR chloride channels (Lacruz et al. 2013; Bronckers et al. 2015).

In conclusion, we have identified the conditions required to obtain an optimally polarized layer of HAT-7 cells, and we have shown that these express the most relevant transport proteins described in maturation ameloblasts in vivo, as depicted in Figure 5G. Our microfluorometric pH_i measurements provided evidence for the presence of the basolateral elements responsible for intracellular bicarbonate accumulation and for regulated basal-to-apical HCO_3^- transport in polarized HAT-7 cells (Fig. 5G). The outcome is therefore a novel experimental model for studying these electrolyte transport processes that are essential for dental enamel formation. However, we must note the limitations of the model. First, as HAT-7 cells are derived from the cervical loop, they

exhibit maturation-stage ameloblast markers but alone cannot sufficiently serve as an optimal maturation ameloblast model. Second, besides bicarbonate transport, additional mechanisms have to be identified, such as active proton transport and TJ functionality, as well as their unknown coordinating mechanisms. Therefore, more complex cell culture models need to be developed (Bhatia and Ingber 2014) in the future for better morphologic and functional modeling of maturation ameloblast function.

Author Contributions

E. Bori contributed to conception and design, data acquisition, analysis, and interpretation, drafted and critically revised manuscript; J. Guo, R. Rácz, B. Burghardt contributed to data acquisition and analysis, and critically revised manuscript; A. Földes contributed to data acquisition, analysis, and interpretation, and drafted and critically revised manuscript; B. Kerémi contributed to data analysis and interpretation, and critically revised manuscript; H. Harada contributed to conception and to data interpretation, and critically revised manuscript; M.C. Steward contributed to design, data analysis and interpretation, and critically revised manuscript; P. Den Besten contributed to conception and design, data interpretation, and critically revised manuscript; A.L.J.J. Bronckers contributed to conception, design, data acquisition, analysis, and interpretation, and drafted and critically revised manuscript; G. Varga, contributed to conception, design, data analysis and interpretation, and drafted and critically revised manuscript. All authors gave final approval and agree to be accountable for all aspects of the work.

Acknowledgments

This study was supported by the National Institutes of Health (National Institute of Dental and Craniofacial Research grant 5R01DE013508, subaward 7743sc), the Hungarian National Development Agency (TÁMOP-4.2.1/B-09/1/KMR-2010-0001, TÁMOP-4.2.2/B-10/1-2010-0013), and the Hungarian Scientific Research Fund (OTKA-NKTH CK-80928). The authors declare no potential conflicts of interest with respect to the authorship and/or publication of this article.

References

Amasheh S, Milatz S, Krug SM, Bergs M, Amasheh M, Schulzke JD, Fromm M. 2009. Na+ absorption defends from paracellular back-leakage by claudin-8 upregulation. Biochem Biophys Res Commun. 378(1):45–50.

Arakaki M, Ishikawa M, Nakamura T, Iwamoto T, Yamada A, Fukumoto E, Saito M, Otsu K, Harada H, Yamada Y, et al. 2012. Role of epithelial-stem cell interactions during dental cell differentiation. J Biol Chem. 287(13):10590–10601.

Baggaley E, McLarnon S, Demeter I, Varga G, Bruce JI. 2007. Differential regulation of the apical plasma membrane Ca(2+) -ATPase by protein kinase A in parotid acinar cells. J Biol Chem. 282(52):37678–37693.

Bardet C, Courson F, Wu Y, Khaddam M, Salmon B, Ribes S, Thumfart J, Yamaguti PM, Rochefort GY, Figueres ML, et al. 2016. Claudin-16 deficiency impairs tight junction function in ameloblasts, leading to abnormal enamel formation. J Bone Miner Res. 31(3):498–513.

Bhatia SN, Ingber DE. 2014. Microfluidic organs-on-chips. Nat Biotechnol. 32(8):760–772.

Bronckers AL, Guo J, Zandieh-Doulabi B, Bervoets TJ, Lyaruu DM, Li X, Wangemann P, DenBesten P. 2011. Developmental expression of solute carrier family 26A member 4 (SLC26A4/pendrin) during amelogenesis in developing rodent teeth. Eur J Oral Sci. 119 Suppl 1:185–192.

Bronckers AL, Lyaruu DM, Guo J, Bijvelds MJ, Bervoets TJ, Zandieh-Doulabi B, Medina JF, Li Z, Zhang Y, DenBesten PK. 2015. Composition of mineralizing incisor enamel in cystic fibrosis transmembrane conductance regulator-deficient mice. Eur J Oral Sci. 123(1):9–16.

Colegio OR, Van Itallie CM, McCrea HJ, Rahner C, Anderson JM. 2002. Claudins create charge-selective channels in the paracellular pathway between epithelial cells. Am J Physiol Cell Physiol. 283(1):C142–C147.

Damkier HH, Josephsen K, Takano Y, Zahn D, Fejerskov O, Frische S. 2014. Fluctuations in surface pH of maturing rat incisor enamel are a result of cycles of H(+)-secretion by ameloblasts and variations in enamel buffer characteristics. Bone. 60:227–234.

Demeter I, Hegyesi O, Nagy AK, Case MR, Steward MC, Varga G, Burghardt B. 2009. Bicarbonate transport by the human pancreatic ductal cell line HPAF. Pancreas. 38(8):913–920.

Harada H, Ichimori Y, Yokohama-Tamaki T, Ohshima H, Kawano S, Katsube K, Wakisaka S. 2006. Stratum intermedium lineage diverges from ameloblast lineage via Notch signaling. Biochem Biophys Res Commun. 340(2):611–616.

Harguindey S, Arranz JL, Polo Orozco JD, Rauch C, Fais S, Cardone RA, Reshkin SJ. 2013. Cariporide and other new and powerful NHE1 inhibitors as potentially selective anticancer drugs: an integral molecular/biochemical/metabolic/clinical approach after one hundred years of cancer research. J Transl Med. 11:282.

Hata M, Kawamoto T, Kawai M, Yamamoto T. 2010. Differential expression patterns of the tight junction-associated proteins occludin and claudins in secretory and mature ameloblasts in mouse incisor. Med Mol Morphol. 43(2):102–106.

Hegyesi O, Foldes A, Bori E, Nemeth Z, Barabas J, Steward MC, Varga G. 2015. Evidence for active electrolyte transport by two-dimensional monolayers of human salivary epithelial cells. Tissue Eng Part C Methods. 21(12):1226–1236.

Hou J. 2014. The kidney tight junction (review). Int J Mol Med. 34(6):1451–1457.

Inai T, Sengoku A, Hirose E, Iida H, Shibata Y. 2008. Differential expression of the tight junction proteins, claudin-1, claudin-4, occludin, ZO-1, and PAR3, in the ameloblasts of rat upper incisors. Anat Rec (Hoboken). 291(5):577–585.

Ishiguro H, Naruse S, Kitagawa M, Suzuki A, Yamamoto A, Hayakawa T, Case RM, Steward MC. 2000. CO2 permeability and bicarbonate transport in microperfused interlobular ducts isolated from guinea-pig pancreas. J Physiol. 528(Pt 2):305–315.

Ishiguro H, Steward MC, Lindsay AR, Case RM. 1996. Accumulation of intracellular HCO3– by Na(+)-HCO3– cotransport in interlobular ducts from guinea-pig pancreas. J Physiol. 495(Pt 1):169–178.

Jalali R, Guo J, Zandieh-Doulabi B, Bervoets TJ, Paine ML, Boron WF, Parker MD, Bijvelds MJ, Medina JF, DenBesten PK, et al. 2014. NBCe1 (SLC4A4) a potential pH regulator in enamel organ cells during enamel development in the mouse. Cell Tissue Res. 358(2):433–442.

Jalali R, Zandieh-Doulabi B, DenBesten PK, Seidler U, Riederer B, Wedenoja S, Micha D, Bronckers AL. 2015. Slc26a3/Dra and Slc26a6 in murine ameloblasts. J Dent Res. 94(12):1732–1739.

Josephsen K, Takano Y, Frische S, Praetorius J, Nielsen S, Aoba T, Fejerskov O. 2010. Ion transporters in secretory and cyclically modulating ameloblasts: a new hypothesis for cellular control of preeruptive enamel maturation. Am J Physiol Cell Physiol. 299(6):C1299–C1307.

Kawano S, Morotomi T, Toyono T, Nakamura N, Uchida T, Ohishi M, Toyoshima K, Harada H. 2002. Establishment of dental epithelial cell line (HAT-7) and the cell differentiation dependent on Notch signaling pathway. Connect Tissue Res. 43(2–3):409–412.

Lacruz RS, Hilvo M, Kurtz I, Paine ML. 2010. A survey of carbonic anhydrase mRNA expression in enamel cells. Biochem Biophys Res Commun. 393(4):883–887.

Lacruz RS, Smith CE, Bringas P Jr, Chen YB, Smith SM, Snead ML, Kurtz I, Hacia JG, Hubbard MJ, Paine ML. 2012. Identification of novel candidate genes involved in mineralization of dental enamel by genome-wide transcript profiling. J Cell Physiol. 227(5):2264–2275.

Lacruz RS, Smith CE, Kurtz I, Hubbard MJ, Paine ML. 2013. New paradigms on the transport functions of maturation-stage ameloblasts. J Dent Res. 92(2):122–129.

Lacruz RS, Smith CE, Moffatt P, Chang EH, Bromage TG, Bringas P Jr, Nanci A, Baniwal SK, Zabner J, Welsh MJ, et al. 2012. Requirements for ion and solute transport, and pH regulation during enamel maturation. J Cell Physiol. 227(4):1776–1785.

Lal-Nag M, Morin PJ. 2009. The claudins. Genome Biol. 10(8):235.

Lee MG, Ohana E, Park HW, Yang D, Muallem S. 2012. Molecular mechanism of pancreatic and salivary gland fluid and HCO3 secretion. Physiol Rev. 92(1):39–74.

Lyaruu DM, Bronckers AL, Mulder L, Mardones P, Medina JF, Kellokumpu S, Oude Elferink RP, Everts V. 2008. The anion exchanger Ae2 is required for enamel maturation in mouse teeth. Matrix Biol. 27(2):119–127.

Matsumoto A, Harada H, Saito M, Taniguchi A. 2011. Induction of enamel matrix protein expression in an ameloblast cell line co-cultured with a mesenchymal cell line in vitro. In Vitro Cell Dev Biol Anim. 47(1):39–44.

Melvin JE, Yule D, Shuttleworth T, Begenisich T. 2005. Regulation of fluid and electrolyte secretion in salivary gland acinar cells. Annu Rev Physiol. 67:445–469.

Rakonczay Z Jr, Fearn A, Hegyi P, Boros I, Gray MA, Argent BE. 2006. Characterization of H+ and HCO3– transporters in CFPAC-1 human pancreatic duct cells. World J Gastroenterol. 12(6):885–895.

Reibring CG, El Shahawy M, Hallberg K, Kannius-Janson M, Nilsson J, Parkkila S, Sly WS, Waheed A, Linde A, Gritli-Linde A. 2014. Expression patterns and subcellular localization of carbonic anhydrases are developmentally regulated during tooth formation. PLoS One. 9(5):e96007.

Schwiebert EM, Zsembery A. 2003. Extracellular ATP as a signaling molecule for epithelial cells. Biochim Biophys Acta. 1615(1–2):7–32.

Smith CE. 1998. Cellular and chemical events during enamel maturation. Crit Rev Oral Biol Med. 9(2):128–161.

Steward MC, Ishiguro H, Case RM. 2005. Mechanisms of bicarbonate secretion in the pancreatic duct. Annu Rev Physiol. 67:377–409.

Szlavik V, Szabo B, Vicsek T, Barabas J, Bogdan S, Gresz V, Varga G, O'Connell B, Vag J. 2008. Differentiation of primary human submandibular gland cells cultured on basement membrane extract. Tissue Eng Part A. 14(11):1915–1926.

Szucs A, Demeter I, Burghardt B, Ovari G, Case RM, Steward MC, Varga G. 2006. Vectorial bicarbonate transport by Capan-1 cells: a model for human pancreatic ductal secretion. Cell Physiol Biochem. 18(4–5):253–264.

Yoshizaki K, Yamamoto S, Yamada A, Yuasa K, Iwamoto T, Fukumoto E, Harada H, Saito M, Nakasima A, Nonaka K, et al. 2008. Neurotrophic factor neurotrophin-4 regulates ameloblastin expression via full-length TrkB. J Biol Chem. 283(6):3385–3391.

Zheng L, Seon YJ, Mourao MA, Schnell S, Kim D, Harada H, Papagerakis S, Papagerakis P. 2013. Circadian rhythms regulate amelogenesis. Bone. 55(1):158–165.